Trans. JWRI, Vol. 25(1996), No.2

Three-Dimensional Simulation of Melting and Evaporation Dynamics by the Unified Solver CIP for Solid, Liquid and Gas

T. Yabe

Department of Energy Sciences, Tokyo Institute of Technology
4259 Natatsuta, Midori-ku, Yokohama 226, Japan

Abstract

We have succeeded for the first time to simulate dynamic phase transition from metal to vapor. This success is due to the CIP method that can treat solid, liquid and gas together and can trace a sharp interface with almost one grid. The code is applied to the formation of crater under the illumination of a short pulse laser. The crater size created by 650mJ laser in 8nsec agrees well with the simulation including an elastic-plastic effect and its depth is 100μm which corresponds to anomalously large cutting speed of 10^6cm/sec for 8ns pulse. However, the simulation demonstrates that evaporation is caused by remnant hot gas during several 100ns and occurs in the direction of 75 degree in an intermittent and unstable manner leading to a unique explanation on the angular distribution of debris. Some example of three-dimensional simulations are also presented.

1. Introduction

The developing speed of computer hardware is quite fast compared to software technology because of various innovations in basic technology. We need similar innovation to accelerate the developing speed of software. One of them will be a universal solver for computational engineering problems. Recent high technology requires new tools for combined analysis of materials in different phase state, e.g., solid, liquid and gas. A universal treatment of all phases by one simple algorithm is essential and we are at the turning point of attacking this goal.

For these types of problems such as welding and cutting processes, we need to treat topology and phase changes of the structure simultaneously. In freezing, condensation, melting and evaporation, the grid system aligned to the solid or liquid surface has no meaning and sometimes the mesh is distorted and even broken up. To solve these problems with Lagrangean representation in finite difference, finite element and boundary element methods will be quite a challenging task.

Toward this goal, we take Eulerian-approach based on CIP[1-3] method developed by the author which does not need adaptive grid system and therefore removes the problems of grid distortion caused by structural break up and topology. The material surface can be captured almost by one grid throughout the computation. Furthermore, the code can treat all the phases of materials from solid state through liquid and two phase state to gas without restriction on the time step from high-sound speed.

In this paper, we will give a historical review of the CIP method and its strategy, then give some examples related to laser interaction cutting process.

Transactions of JWRI is published by Joining and Welding Research Institute of Osaka University, Ibaraki, Osaka567, Japan.

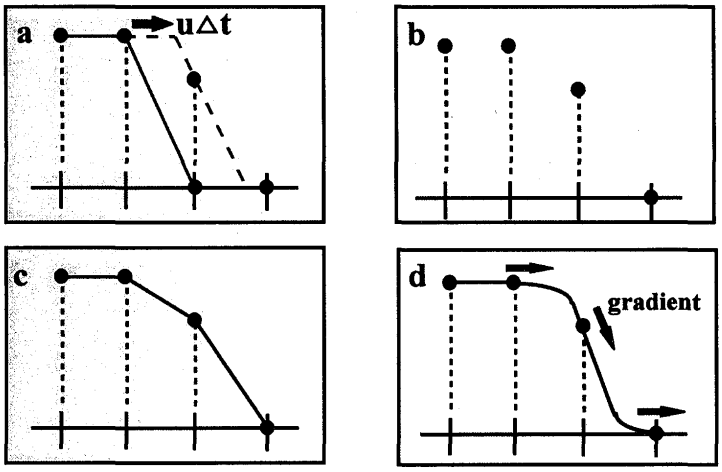

Fig. 1 : The principle of the CIP. (a) solid line is initial profile and dashed line is an exact solution after advection, whose solution (b) at discretized points. (c) When (b) is linearly interpolated, numerical diffusion appears. (d) In the CIP, spatial derivative also propagates and the profile inside a grid cell is retrieved.

2. CIP Method

In order to attack the problems mentioned above, we must first find a method to solve the interaction of compressible gas with incompressible liquid or solid. For compressible fluid, elaborate schemes like TVD or ENO proved to be quit effective in capturing shock waves. However, since these schemes employ a conservative form of fluid equations, divergence of velocity which becomes zero in the incompressible limit cannot be treated independently of the advection part. On the contrary, incompressible schemes like QUICK or higher-order upwind schemes combined with improved MAC (Marker and Cell) procedure can treat divergence-free fluid vorticity and turbulence. However, these schemes cannot always treat shock wave as a sharp discontinuity.

We need a scheme to treat both compressible and incompressible fluids simultaneously in one program to simulate the interaction of gas with liquid or solid. Fully implicit solvers can treat this procedure, but the convergence of iteration in highly distorted state is still a problem.

Recently, we have proposed a new type of scheme CIP[1,2] to treat shock waves by a nonconservative scheme. By a simple extention, the CIP can be used for both compressible and incompressible fluids simultaneously. This code is called the CCUP[3] and can treat incompressible fluid with full hydrodynamic equations. In combination with the surface capturing scheme presented (which will be called "digitizer" here-after) in the previous paper[4], this scheme provides a useful tool to describe various physical processes which were never attacked.

In this section, we review the CIP method illustrate its principle. The key issues of the CIP method are in the representation of advection term and splitted treatment of other terms. By this separation, the code can be extensible to compressible and incompressible fluids. Let us first start with a one-dimensional linear advection equation.

$$\frac{\partial f}{\partial t} + u\frac{\partial f}{\partial x} = 0 \qquad (1)$$

The solution of Eq.(1) gives a simple translational motion of wave with a velocity u. The initial profile (solid line of **Fig. 1** (a)) moves like a dashed line in a continuous representation. At this time, the solution at grid points is denoted by closed circles and is the same as the exact solution. However, if we eliminate the dashed line as in Fig.1(b), it is hard to imagine the original profile and it is natural to retrieve the original profile like that shown by solid line in (c). Thus, numerical diffusion occurred when we construct the profile by the linear interpolation even with the exact solution as shown in Fig. 1(c). This process is the first-order upwind scheme. On the other hand, if we use quadratic polynomial for interpolation, it suffers from overshooting. This process is the Lax-Wendroff scheme or Leith scheme.

What made this solution worse ? This is why

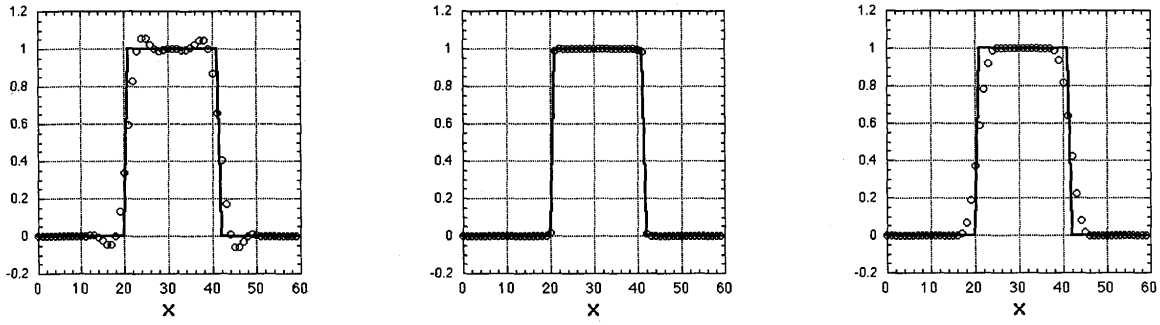

Fig. 2 : A square wave profile after 1000 time steps with CFL=UΔt/Δx=0.2. The solid line is an analytical solution and symbols are numerical solution. (left) original CIP, (center) transformation with tangent function and (right) rational CIP.

we neglect the behavior of the solution inside grid cell and merely follow after the smoothness of the solution. Therefore, we should consider how to incorporate the real solution into the profile within a grid cell. We proposed to approximate the profile as shown below. Let us differentiate Eq.(1) with spatial variable x, then we get

$$\frac{\partial g}{\partial t} + u\frac{\partial g}{\partial x} = -\frac{\partial u}{\partial x} g \qquad (2)$$

where g stands for the spatial derivative of f, $\partial f/\partial x$. In the simplest case where the velocity u is constant, Eq.(2) coincides with Eq.(1) and represents the propagation of spatial derivative with a velocity u. By this equation, we can trace the time evolution of f and g on the basis of Eq.(1). If g propagates as shown in Fig. 1(d), the profile after one step is limited to a specific profile. It is easy to imagine that by this limitation, the solution becomes very closer to the initial profile.

If two values of f and g are given at two grid points, the profile between these points can be described by cubic polynomial $F(x)= ax^3+ bx^2+cx+d$. Thus, the profile at n+1 step can be obtained shifting the profile by $u\Delta t$ like $f^{n+1}+1.F(x-u\triangle t)$, $g^{n+1}=dF(x-u\triangle t)/dx$.

$$f_i^{n+1} = a\xi^3 + b\xi^2 + g_i\xi + f_i$$
$$g_i^{n+1} = 3a\xi^2 + 2b\xi + g_i$$
$$a = \frac{g_i + g_{iup}}{D^2} + \frac{2(f_i - f_{iup})}{D^3}$$
$$b = \frac{3(f_{iup} - f_i)}{D^2} - \frac{2g_i + g_{iup}}{D} \qquad (3)$$

where we define ξ=-u $\triangle$ t and D=-sgn(u)Δ x, iup=i-sgn(u), since the upward direction depends on the sign of the velocity(=sgn(u)). An interpolation with f and its derivative is called Hermite spline. However, the key issue of the CIP scheme is in the way of determining the time evolution of spatial derivative. We proposed to determine them from spatial derivatives of Eq.(1) also. Therefore, the profile even within a grid cell is determined so as to be consistent with the equation.

By repeating Eq.(3), we can get the solution of Eq.(1). One example is shown in **Fig. 2** (left). A small overshooting is unavoidable but does not grow in time. In most of practical calculation, this quality is sufficient. However, for the description of the sharp interface, we need more accurate solution. We proposed two methods to improve the solution.

2.1 Digitizer

In some special cases, one need to treat sharp interface with exactly one grid. There have been numerous methods proposed for treating interface between two different materials. These methods are divided into two groups. In one group the interface is described by a surface function, while in the other group the interface is defined as surface of a density function[5] such as VOF (Volume of Fluid Method). In the former case, main problem arises from a multi-valued function when the surface is strongly distorted or even breaks up. Although this shortcoming will not arise in the latter case, the numerical scheme to describe an evolution of the density function without numerical diffusion is a problem which needs further investigation. The level set

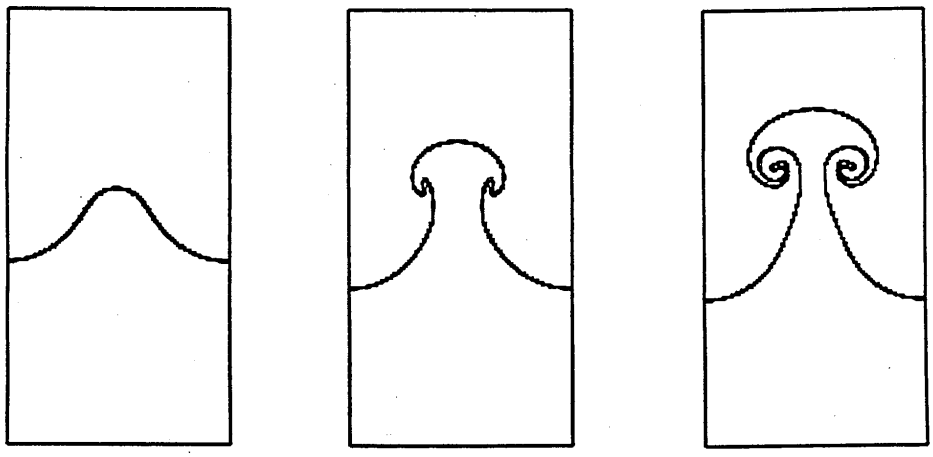

Fig. 3 : Injection of heavier liquid into lighter liquid. Equally-spaced 180×90 Cartesian fixed grids are used.

function[6] is another interesting example of the latter case and is worthy of further investigation.

Recently, we proposed a simple method[4,7] to treat the density function ϕ with high accuracy in multi-dimension. For this purpose, we slightly modified the CIP method described above. We proposed to transform ϕ into $F(\phi)$. It is obvious that a new function $F(\phi)$ also obeys the same equation as the density function if it is monotone function of ϕ. We can choose an appropriate function to ensure monotone and sharp dis-continuity. In the previous paper, we chose the tangent function:

$$F(\phi) = \tan\left[\pi\left(\phi - \frac{1}{2}\right)\right] \qquad (4)$$

and the equation for F

$$\frac{\partial F}{\partial t} + u\frac{\partial F}{\partial x} = 0 \qquad (5)$$

is solved. It should be noticed that the equation to be solved for the spatial derivative is the derivative of Eq.(5) but is not of Eq.(1) because the target equation is now Eq.(5). In all the time steps, only F and its derivative $\partial F/\partial x$ are calculated and then if it becomes necessary, ϕ is obtained by the inverse transformation of Eq.(4). The result with this scheme is shown in Fig.2(center), where no overshooting appears and very small diffusion is attained. This is clear from the definition of tangent function.

This tangent function is useful to represent the interface by the density function in which only digitized values 0 and 1 appear. This scheme is applied to the injection of heavier fluid into lighter fluid. In this case, we set the sound speed to quite a large value and hence the process treated here is almost incompressible although full hydro-dynamic equations is used with the method described in section 3. The result is shown in **Fig.3**. The interface of two fluids has successfully been treated by one grid throughout the computation.

2.2 Rational Function CIP

Although the digitizer is useful for density function or for incompressible fluid, we meet the problem where density can change in time in each region separated by sharp interface. Although we can use the same technique even in this case[4], we had better consider more elaborate method to eliminate overshooting. We may use MmB scheme or limiter function. However, we prefer to use the rational function:

$$F(x) = \frac{ax^3 + bx^2 + cx + d}{1 + \alpha Bx} \qquad (6)$$

where α is the switching parameter. If α is 0, Eq.(6) is merely the CIP method. When α is 1, it can be convex-concave preserving scheme when the coefficients are given by

$$a = \left[g_i - S + (g_{iup} - S)(1 + \alpha BD)\right]/D^2$$

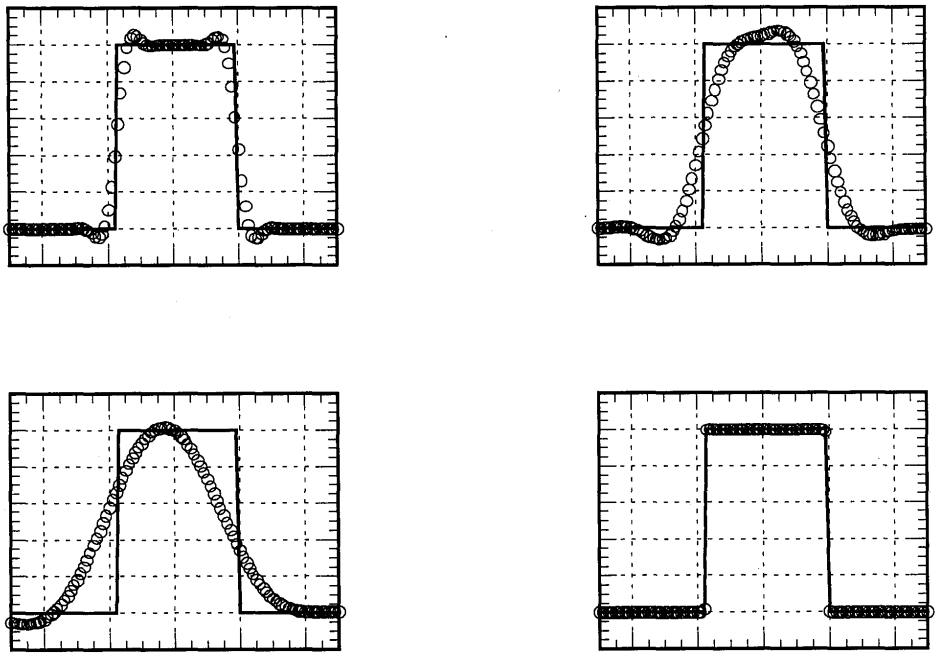

Fig. 4 : The result with implicit CIP. (left-top) CFL = 0.5, (right-top) CFL = 4.0, (left-bottom) CFL = 10and (right-bottom) CFL = 4with digitizer.

$$b = S\alpha B + (S - g_i)/D - aD$$
$$c = g + f\alpha B, \quad d = f_i$$
$$B = \left[\left|(S - g_i)/(g_{iup} - S)\right| - 1\right]/D$$
$$S = (f_{iup} - f_i)/D \qquad (7)$$

where D and iup are already defined in Eq.(3) (see Ref[8,9] for details). As shown in Fig.2(right), monotone and convex-concave preserving scheme is attained.

2.3 Implicit CIP

Another interesting modification of the CIP method is its implicit version[10]. Although it is implicit, it is directly solved in non-iterative way. In obtaining Eq.(3), we shift the profile from the past to the present. On the contrary, the profile is shifted from future to the present in the implicit scheme. Therefore, we can replace f and g by f^{n+1} and g^{n+1}, and change ξ to be $-\xi$. Rearranging this result, we obtain the expression:

$$f_i^{n+1} = (k+1)^{-3}\left[-k(k+1)(kg_{iup}^{n+1} - g_i^n)D + k^2(k+3)f_{iup}^{n+1} + (3k+1)f_i^n\right]$$
$$g_i^{n+1} = (k+1)^{-3}\left[(k+1)\{(k-2)g_{iup}^{n+1} - (2k-1)g_i^n\} + 6k(f_{iup}^{n+1} - f_i^n)/D\right]$$
$$k = -u\Delta t/D \geq 0 \qquad (8)$$

Fortunately, only two points are connected in the CIP method. For example, j and j-1 are related in case of u>0. Therefore, even in the implicit solution, we can directly solve it from the upwind direction. It is easy to extend it to the case where velocity changes its sign[4]. **Figure 4** shows the result and demonstrates its stability and correctness. Surprisingly, combination of digitizer with implicit scheme gives a very accurate result even for $u\Delta t/\Delta x = 4$.

3. Application to Hydrodynamics

We use full hydrodynamic equations for both compressible and incompressible fluids, which can be written in a form:

$$\frac{df}{dt} \equiv \frac{\partial f}{\partial t} + (\mathbf{u}\cdot\nabla)\mathbf{f} = \mathbf{g}, \qquad (9)$$

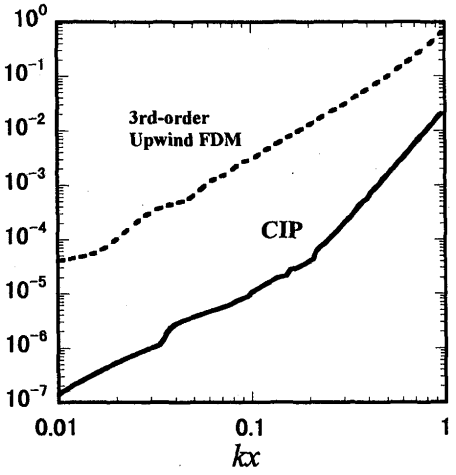

Fig. 5 : The conservation error when the velocity profile $u(x)=1+0.5\sin[2\pi(x-1)/270]$ is used. The error=sum of ρ)/(sum of initial ρ)$\times$100%. 270 is the number of grids. Old : non-advection first and advection second. New : advection first (Courtesy of T. Aoki).

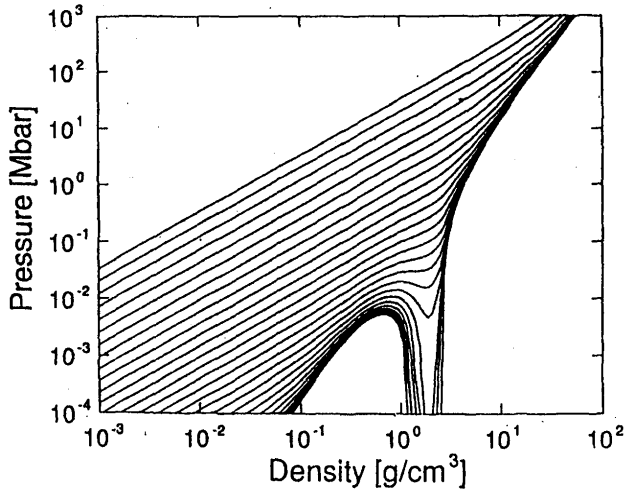

Fig. 6 : Equation of state of aluminum.

where $\mathbf{f}=(\rho, \mathbf{u}, E)$ and $\mathbf{g}=(-\rho\nabla\cdot\mathbf{u}, -\nabla P/\rho, +Q_U, -P\nabla\cdot\mathbf{u}/\rho+Q_E)$, where ρ is the density, $\mathbf{u}$ the velocity, P the pressure, E the specific internal energy, Q_U represents viscous and stress terms, and Q_E includes viscous heating, heat conduction and heat source.

The CIP method solves the equations like Eq.(9) by dividing those into non-advection and advection phases. A cubic-interpolated profile is shifted in space in the advection phase as shown in the previous sections. Then, the non-advection phase can be solved with finite difference or finite volume method. It would be useful to show the conservative property in this procedure. **Figure 5** shows an error occurred when Eq.(9) with scalar variable ρ is solved under the given oscillating velocity field. We should remind here that conservative property increases when the order of calculation is changed.

As shown in the previous papers, we can trace shock waves correctly with the CIP method although it uses fluid equations written in a non-conservative form. This success is due to the high accuracy of the CIP method and an improved artificial viscosity[11]. Since we are treating hydrodynamic equations in a non-conservative form, it is easy to extend it to include both incompressible and compressible fluids Let us consider again the origin of the difficulty. In the **Fig. 7**, we plot the iso-temperature contour of Aluminum automatically generated from the semi-analytical formula. In the gas phase where density is sufficiently low, the pressure is in proportion to the density. Therefore, we may solve the density first in Eq.(9) and then after temperature is obtained, we use EOS(equation of state) in **Fig. 6**. However, near the solid density of 2.7g/cm^3, the pressure rises very sharply. If we use the same procedure there, the pressure can change easily by 3-4 orders of magnitude even with small error of density around few tens of percent. Therefore, the strategy to solve the density first is broken in this area. This is the reason why the universal treatment of solid, liquid and gas is a difficult task. In attacking this problem, the physicist in incompressible fluid invented an interesting technique. We will translate the strategy they used from a different view point and reconsider the technique. If the pressure is very sensitive to the density, we had better solve pressure at first. This means that we should rotate Fig.6 by 90 degree. If we have a way to solve pressure at first, then we get density very accurately at the solid density. Since the pressure is proportional to density in the gas phase, this strategy does not harm the solution there either. Then how to realize this strategy ? Our method starts with the thermodynamic relation:

$$\Delta p=\left(\frac{\partial p}{\partial \rho}\right)_T \Delta\rho+\left(\frac{\partial p}{\partial T}\right)_P \Delta T \qquad (10)$$

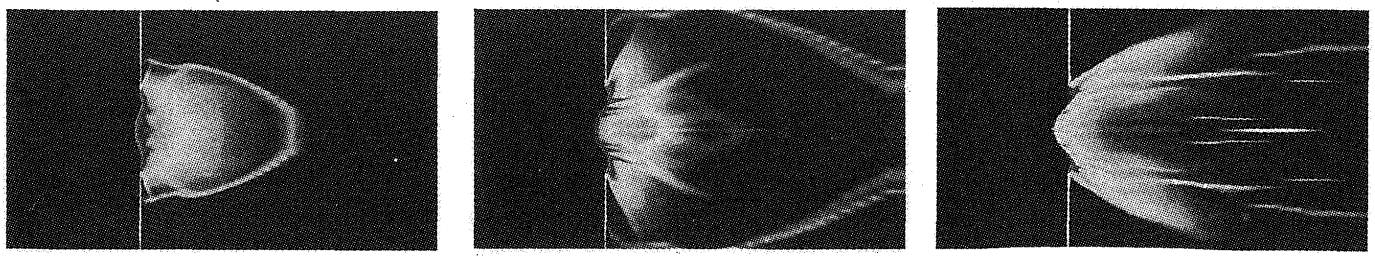

Fig. 7 : Density contour of aluminum illuminated by laser light. Time sequence is 50, 100, 300 nsec. Filamentary structure explains the experimental results.

where $\triangle p = p^{n+1} - p^*$ and represents profile after advection. The same expression is used for ρ and T. Therefore, if $\Delta\rho$ and ΔT are predicted, ΔP can be obtained since $\partial p/\partial\rho$, $\partial p/\partial T$ are already given from EOS. The advantage of the CIP is the separate treatment of the non-advection term. Therefore, we can limit our discussion here to the non-advection term only. We should note that this merit is quite important to get the final result. Then we get

$$\Delta\rho = -\rho^* \nabla \cdot \mathbf{u}^{n+1} \Delta t$$
$$\rho^* C_V \Delta T = -P_{TH} \nabla \cdot \mathbf{u}^{n+1} \Delta t \qquad (11)$$

where C_V is the specific heat for constant volume. The velocity $\mathbf{u}^{n+1}$ in above equations can be eliminated by using the equation of motion:

$$\Delta \mathbf{u} = -\frac{\nabla p^{n+1}}{\rho^*} \Delta t \qquad (12)$$

($\triangle \mathbf{u} = \mathbf{u}^{n+1} - \mathbf{u}^*$) we obtain the equation for p^{n+1} [3.12)]

$$\nabla\left(\frac{1}{\rho^*}\nabla p^{n+1}\right) = \frac{p^{n+1} - p^*}{\Delta\left(\rho C_S^2 + \dfrac{p_{TH}^2}{\rho C_V T}\right)} + \frac{\nabla \cdot \mathbf{u}^*}{\Delta t} \qquad (13)$$

where $P_{TH} = T(\partial p/\partial T)_\rho$ 、 $Cs^2 = (\partial p/\partial\rho)_T$.

Thus velocity $\mathbf{u}^{n+1}$ can be calculated by Eq.(12) and then the density ρ^{n+1} is by Eq.(11). It is very important to note that in Eq.(13), ρ is inside the derivative on the left-hand side. At the interface between materials having large density difference, the continuity of acceleration $\nabla p/\rho$ is very important because the denominator ρ can change by several orders of magnitude in one grid. Equation (13) guarantees the continuity of $\nabla p/\rho$ for incompressible ($\nabla \cdot u = 0$) and steady state. By this procedure, we can treat all the material at once by simply changing its equation of state. We note again that this property is a consequence of the separate treatment of advection and non-advection terms, otherwise the continuity of $\nabla p/\rho$ is not guaranteed and a large density can not be traced.

Figure 7 shows melting and evaporation of aluminum under the illumination of laser light, where the density changes from 2.7 to 10^{-4} g/cm^3. Aluminum solid is treated as an elastic-plastic material initially and then changes to liquid and vapor during phase transition. This change is simply realized by the equation of motion. This example shows the high ability of the code to describe a sharp interface and to be robust enough to treat both compressible and incompressible fluid simultaneously.

The experiment was performed at the Institute of Laser Engineering, Osaka University regarding the x-ray source development[6]: a YAG laser of 650mJ in 8nsec is used to obliquely illuminate an aluminum slab target with an angle of 45degree to the target normal. Final crater depth and shape agree quite well with the simulation in **Fig. 8** and seems to be anomalous because the cutting speed is 100 μm/ 8nsec$\sim$ 10^6cm/sec if this crater should have been created during laser pulse. Since the speeds of sound wave and elastic wave inside aluminum are order of 10^5cm/sec, the cutting speed is much larger than these speeds. Is this speed physically possible? It is interesting to note that the crater is not formed during the laser pulse, but it develops gradually in the time scale of several

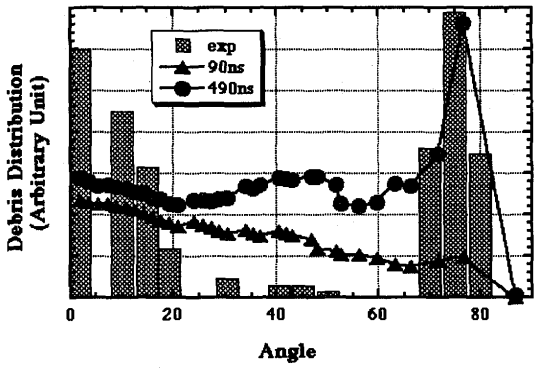

Fig. 8 : Debris distribution. 0 degree corresponds to the target normal. The histogram shows the experimental result, while circles and triangles show the accumulated mass from the simulation at 490ns and 90ns, respectively.

100ns well after the laser pulse ended as shown in Fig.8. The very high temperature plasma more than a few tens of eV produced by the 8ns laser pulse and most of them expands from the target. However, some of them still stay near the target for long time after the laser pulse because of recoil force from expanded plasmas and act as heat source to melt aluminum metal in the time scale of several 100ns.

When the plasma temperature becomes less than melting temperature around 290nsec (the time is measured from the laser peak) , the stress of aluminum whose strength is 0.248Mbar and yield strength is 2.2976kbar is recovered and no distortion occurs after that time. This yield stress is quite important to determine the final crater size. Without yield strength, the crater develops further even after 490ns and the depth becomes more than 300 μm although less difference is seen at the beginning around 90ns.

The plasma heated crater formation leads to other interesting phenomena. Since the plasma acts not only as heat source but also as pressure source, the dynamic expansion of evaporated material at later time is strongly modified. Since a high pressure region is just in front of the evaporation surface, the vapor is forced to flow bypassing through a narrow channel between the metal surface and this pressure source. Therefore, the vapor preferentially flows toward a circumference with a large angle to the target normal. This effect is the exactly the same as that obtained in the experiment. Figure 8 shows a distribution of debris from the targets. The histogram is the experimental result and it was drawn from 2000shots accumulated. Clearly there exist two peaks around O and 75degree. As in Fig.7, the plasma expands directed normally to the target at early time t<90 ns and this expansion is a bulk part of the laser-heated plasma. As already stated, this expansion causes recoil force to the hot plasma surrounding aluminum surface. This main part of the expansion creates a peak at O degree. The triangles in **Fig.9** show the distribution calculated from the time integration of mass flow ρ u up to t=90ns. At an early stage t<90ns, no peak appears around 75degree. On the other hand, the expansion at later stage t>90nsec is limited to the sideward direction as stated before and creates the peak at 75degree. Therefore accumulated distribution up to 490ns shown by circles in Fig.8 increases mainly at 75degree.

Simulation also predicts further interesting behavior. The expansion at t<40nsec is quite uniform because its temperature is quite high $\sim$ a few tens of eV. The experiment supports this result and the debris around 0 degree is very fine and indistinguishable with an optical microscope. On the other hand, the simulation result at t=290nsec shows some filamentary streams flowing from the surface. The experiment also supports this result and the debris at 75degree consists of 1 to 20 μm sized particles. Since the simulation is two-dimensional axisymmetric, we cannot estimate the particle size but we can suggest the origin of the filaments.

The evaporated gas at later time must flow through a very narrow channel to the circumference and therefore this narrow channel creates thermal insulation layer between metal surface and heat source. Then heat flow is instantaneouly suppressed reducing evaporation. If the evaporation is suppressed, the narrow channel disappears and the heat source directly contact the metal surface. Thus the heat flow from heat source to metal surface is recovered causing again evaporation and the formation of narrow channel of thermal insulation layer. Repeating this process, the intermittent evaporation occurs and the filamentary streams appear as shown in Fig.7. Although the detailed time evolution is not seen from Fig.7, the animation picture shows that, during flight to vacuum, condensation occurs from low density clouds to well defined filaments seen in Fig.7 at 290ns.

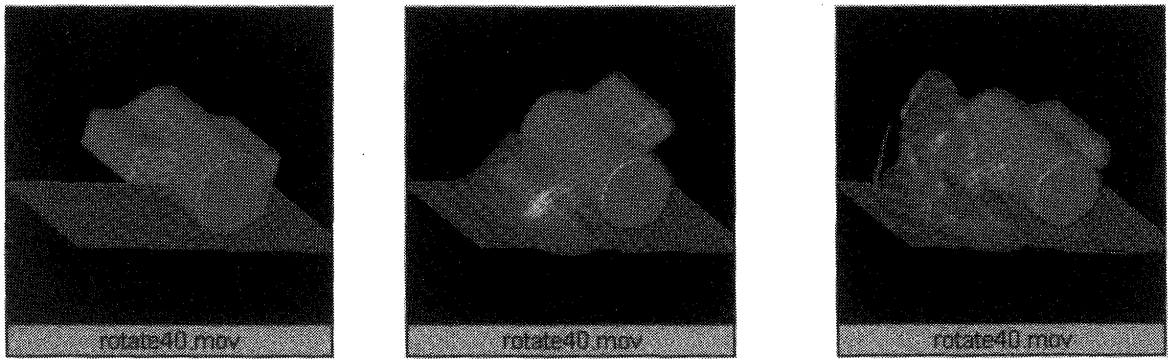

Fig. 9

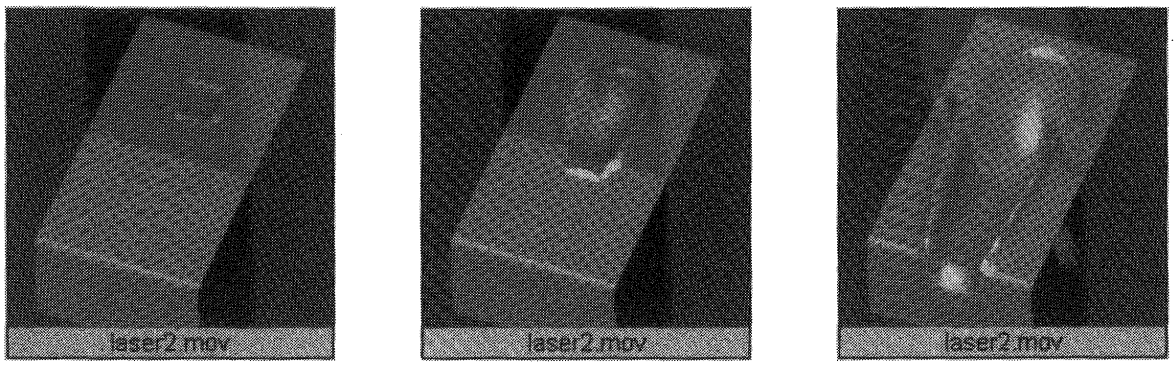

Fig. 10

4. Three-Dimensional Results

There are many applications of this scheme. We will show here some of the typical examples. One of the features of the code is the high ability to trace an interface. In all the simulations given in this paper have been performed in a Cartesian fixed grid system. In Fig.9, a solid rotar is rotating just above the water surface. In **Fig. 10**, acrylic block is illuminated by $C0_2$ laser whose spot is moving from top-right to bottom-left in time by scanning a surface. In the middle, we also plot density contour to show behavior of the evaporated gas.

References

[1] H.Takewaki, A.Nishiguchi and T.Yabe : J. Comput. Phys. 61 (1985) P.261.
[2] T.Yabe et al. : Comput.Phys.Commun. 66 (!991) P.219.
[3] T.Yabe and P.Y.Wang : J.Phys. Soc.Japan ,60 (1991) P.2105.
[4] T.Yabe and F.Xiao : J.Phys. Soc. Japan 62 (1993) P.2537.
[5] C.W.Hirt and B.D.Nichols :J.Comput.Phys. 39 (1981) P.201.
[6] S.Osher and J.A.Sethian :J.Comput.Phys. 79 (1988) p. 12
[7] F.Xiao and T.Yabe : Shock Waves 4 (1994) P IOI.
[8] F.Xiao, T.Yabe and T.Ito : Comput.Phys. Commn. 93 (1996) p. I.
[9] F.Xiao et al. : Comput.Phys.Commn. 94 (1996) p.103.
[10] M.Ida and T.Yabe : Comput.Phys. Comm. 92 (1995) P.21.
[11] T.Yabe and F.Xiao : Nucl.Eng. &Design 155 (1995)p.45.
[12] F.Xiao et al. : Comput. Model. & Sim. Eng.1 (1996) P.235.
[13] T.Yabe et al. : Research Report NIFS (National Institute for Fusion Science) Series, NIFS-417, May(1996).